Hindawi
International Journal of Rotating Machinery
Volume 2019, Article ID 1791830, 11 pages
https://doi.org/10.1155/2019/1791830

Research Article

Investigation on Lubrication State of Sliding Bearings in Low-Speed Rotor System Subjected to Torque Load

Xinyu Pang, [1,2] **Wangwang Jiang**, [1,2] **and Xiaowu Jin** [3]

[1] *College of Mechanical and Vehicle Engineering, Taiyuan University of Technology, Taiyuan 030024, China*
[2] *Shanxi Key Laboratory of Fully Mechanized Coal Mining Equipment, Taiyuan 030024, China*
[3] *Qingdao Haier Co., Ltd., Qingdao 266101, China*

Correspondence should be addressed to Xinyu Pang; typangxy@163.com

Received 4 April 2019; Revised 2 June 2019; Accepted 10 June 2019; Published 1 July 2019

Academic Editor: Hyeong Joon Ahn

In order to study the influence of torque load on the lubrication and wear of the sliding bearing of the rigid rotor system, the theoretical and experimental researches on the single-span rotor system with low speed were carried out. A special force sensor was used to measure the bearing load under different torque excitations, and the oil film pressure was calculated. The oil film pressure and thickness of sliding bearing under low speed (210r/min) were simulated by combining the lubrication theory. Based on the film thickness ratio theory, the corresponding relationship between the lubrication state and the torque load value was deduced. In addition, the wear rate and abrasive grain morphology of sliding bearing with different torque values were analyzed by means of oil sample preparation to verify this correspondence. The results show that the film thickness ratio has a logarithmic function relationship with the constant torque load, and the film thickness ratio curve can be used to determine the corresponding torque values under different lubrication states. The wear rate under mixed lubrication state increases exponentially with the torque load, and the main wear mechanism is adhesive wear and abrasive wear. The research results have certain guiding significance to the adjustment of the actual running condition of sliding bearing and its life prediction.

1. Introduction

For large-sized rotating machines such as steam turbines, kinematic pairs between journals and bearings are sliding friction pairs, and the frictional wear of friction pairs directly affects the operating performance of rotor systems. Affected by installation errors, load changes, and other factors, the rotor system is subjected to torque during operation, and torque changes will lead to variations in bearing loads of the system, which will influence the unit stability and safety. Under torque loads, the axis position of the shaft and the lubrication state of journal-bearing will change [1, 2], and the bearing load, oil film pressure, and oil film thickness will change with torque loads [3]. When the minimum oil film thickness is less than the allowable value, the shaft and bearing will be subjected to instantaneous frictional impact, leading to the wear of the friction pair of journal-bearing and jamming, burning, and even damage and casualties in serious cases.

The lubrication state of the sliding bearing is a hot topic at home and abroad. Litwin [4] analyzed the edge bushing wear of water-lubricated bearings in the fluid lubrication state and proposed a new method for calculation of sliding bearing capacity. Dai et al. [5, 6] studied the friction and wear behavior, particle shape, and service life of pivot jewel bearing in oil-bath lubrication under high rotating speed. Sander et al. [7] studied the wear of sliding bearings under dynamic edge loads. Chasalevris et al. [8] built two bearing clearances by applying additional harmonics on excitation systems of magnetic suspension bearings in order to detect sliding bearing wear. Zhu et al. [9] tested and monitored the wear of main journal bearings of diesel engines by the thermoelectric method on the sliding bearing test bench. Bromaghin et al. [10] developed a custom test tank that can simulate on-site deployment and studied the wear rates of various sliding bearings in 60h clean water tests. Bartel et al. [11] introduced a model for calculation of the instantaneous wear of sliding bearings subject to mixed friction. Sano et al. [12] proposed a method for theoretical analysis of sliding bearing wear under mixed lubrication conditions, in which the wear depth of bearing surfaces is calculated according to the EHL theory and surface roughness theory. Nikolakopoulos and Papadopoulos [13] established a sliding bearing wear analysis, which can be applied to study the relationship between friction, angle of displacement, wear depth, and wear-related power consumption. Wu et al. [14] studied the wear mechanism of sliding bearings involving various moisture contents and rotating speeds. Comparative experimental studies on the friction properties and wear mechanism of different materials of sliding bearings under different working conditions have also been studied [15–18].

Chen et al. [19, 20] studied the influence of limit parameters, capillary limit and bearing eccentricity, on the stability of rigid rotor-hybrid bearing system and obtained the optimal parameters of hybrid bearing design. Karkkainen et al. [21] studied the dynamics of the rotor supported by the active magnetic bearing during the lowering of the cage bearing and the effect of misalignment of the cage bearing during the lowering of the rotor. Li et al. [22] established an electromagnetic force model for the misalignment of the cage bearings and studied the effects of bearing misalignment on the stiffness, damping, and damping ratio of the active magnetic bearing (AMB) system. Lu et al. [23] developed a model to predict the effects of misalignment on the static performance of Hydrodynamic-Rolling Hybrid Bearing (HRHB) to provide design guidelines for machining and assembly tolerances. Fu et al. [24] simulated the lubrication characteristics of sliding bearings with different clearance ratios, eccentricity and aspect ratio, and proposed a bearing optimization design method based on the distribution law of lubrication characteristics of sliding bearings.

Some scholars have studied changes in loads of bearings subject to torque loads. Yuan et al. [25] analyzed the effect of constant torque loads on the single-span double-disc rotor system through simulation and experiment combination based on the measured loads. Zhang et al. [26] identified torque disturbance faults of rotor systems based on bearing loads. Pang and Yang [27] studied the coupled vibration responses caused by load changes of one support to the other supports in a multisupport rotor-bearing system. Song et al. [28] studied the effects of various torque loads on the bending characteristics of rotor systems, taking into account the impact of bearing loads. Sun et al. [29] studied the law of axis changes of rotor systems subjected to abrupt torque loads, considering the effects of torque loads on bearing loads.

In order to monitor and analyze the load, lubrication, and wear state of sliding bearings, facilitate the safe operation of equipment, and prolong the service life of equipment, current studies on the lubrication states of sliding bearings mainly focus on the measurement of wear and the impact of rotating speeds and lubricant doses on wear, but little on the impact of torque loads on the lubrication states and wear volumes of sliding bearings. The wear particles generated in wear, fatigue, and corrosion are important information carriers of bearing wear. They can be directly collected from lubricating oil samples and easily monitored in a real-time manner. This paper, based on the single-span double-disc rotor test bench, studies changes in the bearing load, oil film pressure, and oil film thickness of sliding bearings of rigid rotor systems under constant torque loads and identifies the lubrication states of sliding bearings under constant rotating speeds and torque loads based on the film thickness ratio. In addition, this paper studies the effect of torque loads on wear volumes of sliding bearings through ferrography of the collected oil samples to provide a theoretical basis for further prediction of the wear and residual life of sliding bearings under torque loads.

2. Research Plan

2.1. Composition and Parameters of Test Device. The single-span rotor test bench, as shown in Figure 1, consists of the appropriate motor (Y180M-2), elastic pin coupling, rotating shaft (40Cr), disc, sliding bearings I and II (ZQSn6-6-3), bearing force transducer (GYL-9B004), magnetic powder brake (CZ-10), torque-speed sensor (ORT-803), bearing block, and lubrication system.

The rotating speed, acceleration/deceleration time, stable running time, and start/stop of the motor are controlled by a Fuji frequency converter (5000G11S). The motor and rotating shaft are connected via the elastic pin coupling, both ends of the disc are supported by the sliding bearing, and the bearing force transducer between the sliding bearing and bearing block are used for collecting load information of supports of the rotor system under different torque loads. The magnetic powder brake is used for applying torque loads on the rotor system, and the torque is controlled by the tension controller (LTC-002). The rotating shaft, torque-speed sensor, and magnetic powder brake are connected via the elastic pin coupling. The wear of the sliding bearing of the rotor system is sampled in the lubricating oil outlet line. The performance parameters of the sliding bearing, rotating shaft, and lubricating oil are shown in Table 1. Table 2 shows the details of some sensors.

2.2. Technical Route. The technical route for studying on the lubrication state of the sliding bearing of the low-speed rotor system subjected to a constant torque is shown in Figure 2. The sliding bearing II was studied as object in this paper. The program controller controls the magnetic powder brake to apply five kinds of constant torque excitations of 7.2Nm, 21.3Nm, 42.4Nm, 63.2Nm, and 81.5Nm on the rotating shaft. After the rotor system is stably operated, bearing load under different torque excitations is collected by a bearing force transducer installed under the sliding bearing seat, and the oil film thickness and pressure were obtained. Based on the film thickness ratio, the lubrication state of the sliding bearing under different torque excitations is judged, and the corresponding relationship between the torque excitation and the lubrication state is derived.

In order to verify the correctness of this correspondence, the oil samples flowing through the friction bearing of the sliding bearing under different torque excitations were extracted, and the wear, wear rate and abrasive grain shape of the sliding bearing under different torque excitations were further analyzed by spectrum and weighing.

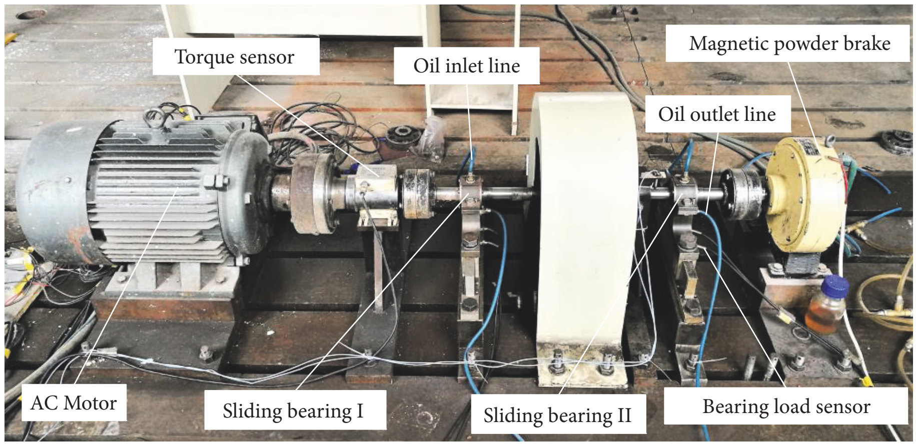

Figure 1: The single-span double-disc rotor test bench.

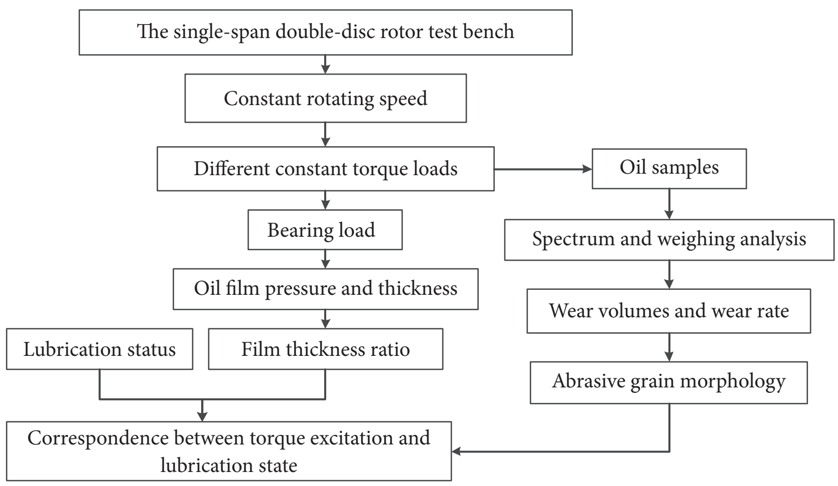

Figure 2: Technical route.

Table 1: The performance parameters of the sliding bearing, shaft, and lubricating oil.

Name	Symbol	Value
Bearing length	L	24 mm
Bearing radius	R	16 mm
Radius gap	C	0.02 mm
Oil supply temperature	T	20°C
Lubricant type	- -	L-TSA32
Rotor and disc mass	m	55.3 kg
Shaft length between two bearings	l	584 mm
Lubricating oil viscosity	η	0.0273 Pa•s(20°C)
Lubricating oil density	ρ	865 kg/m^3

2.3. Measurement of Bearing Load. The bearing force transducer was used to measure loads on the sliding bearing of the rotor system under different torque loads. Figure 3 shows the structural diagram of the load sensor; the sensor is a resistance strain sensor, in which R_1, R_2, R_3, and R_4 are resistance strain gauges bonded at 45° and 135° in four blind holes on the upper short beam of the sensor, for measurement of vertical direction (Y) loads of the bearing; and R_5, R_6, R_7, and R_8 are resistance strain gauges bonded at 45° and 135° in four blind holes on the lateral short beam, for measurement of horizontal direction (X) loads of the bearing. All the above 8 resistance strain gauges are wire strain gauges. When the bearing load changes, the strain gauge will deform, and its resistance value will change. Through the full-bridge circuit, the load changes of sliding bearing in X and Y directions are converted into the change of resistance values and further

Table 2: Sensors details.

Name	Type	Parameter
Bearing force transducer	GYL-9B004	Power supply: ±10V DC Range in the X direction: 0~750Nm Range in the Y direction: 0~2000Nm
Torque-speed sensor	ORT-803	Torque accuracy: < ±0.3%F•s Frequency response: 100μs Nonlinearity: < ±0.2%F•s Operating temperature: -20~70°C

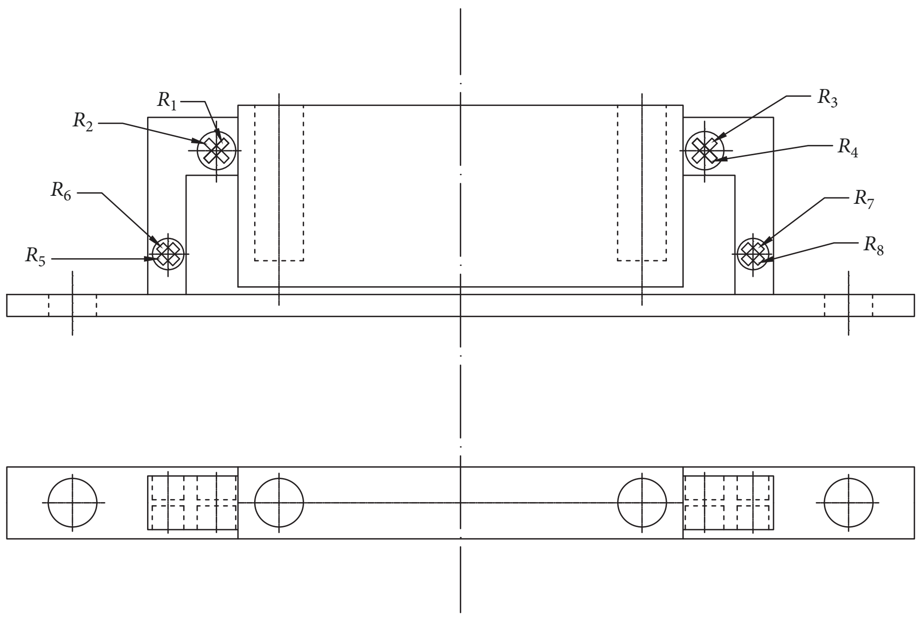

Figure 3: The bearing load sensor.

Table 3: Load value of sliding bearing II under constant torque excitation.

Torque value (Nm)	Load value of sliding bearing II	
	F_x (N)	F_y (N)
0	269.5	391.8
7.2	270.8	398.2
21.3	520.8	852.5
42.4	692.7	1288.9
63.2	808.5	1624.6
81.5	906.5	1878.5

output in the form of voltage values, so as to measure the force status of sliding bearing under torsion.

In order to analyze the impact of five torque loads (7.2 Nm, 21.3 Nm, 42.4 Nm, 63.2 Nm, and 81.5 Nm) on the load of the sliding bearing, the average loads on the sliding bearing II under different torque loads were measured and calculated, as shown in Table 3. It can be seen that, under different torque loads, the load on the sliding bearing of the rotor system rises with the torque value increasing.

3. Lubrication State of Sliding Bearing under Torque Load

3.1. Oil Film Thickness. The schematic diagram for calculation of the oil film thickness of the sliding bearing of the rotor system is shown in Figure 4, where O_b is the center of the sliding bearing, O_j is the center of the rotating shaft, e is the eccentricity, ϕ is the offset angle (i.e., angle between the negative half-axis of the y-axis in the counterclockwise direction and the connecting line of the rotating shaft center and bearing center), A is a point in the axial direction of the bearing, and θ is the angle between the negative half-axis of the y-axis in the counterclockwise direction and the calculation point A. The oil film thickness (h) at the point A is

$$h = C + e\cos(\theta - \phi) \tag{1}$$

where C is radius gap, C=R-r, R is radius of the sliding bearing, and r is radius of the rotating shaft.

The oil film thickness reaches the maximum value in the case of $\theta = \phi$ and minimum value in the case of $\theta = \pi + \phi$.

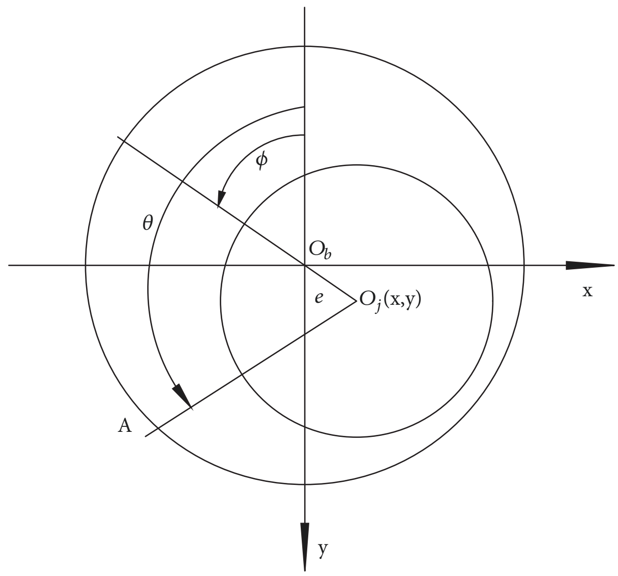

FIGURE 4: The schematic diagram for calculation of oil film thickness of sliding bearing.

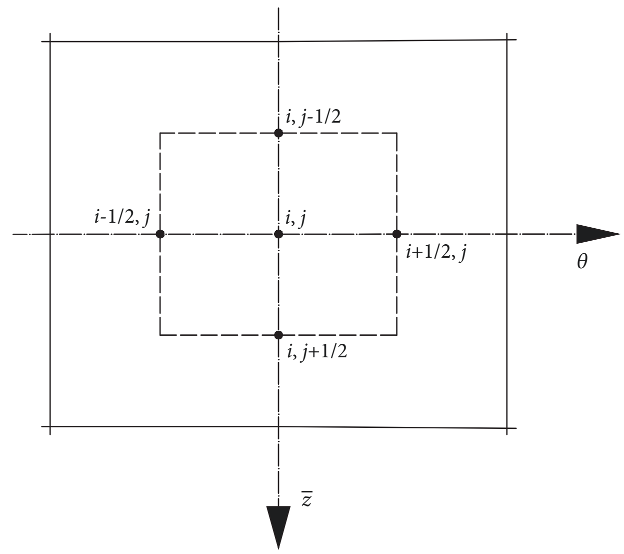

FIGURE 5: Grid division of sliding bearing.

Given that the center coordinates of the rotating shaft are (x, y), the eccentricity is $e = \sqrt{x^2 + y^2}$, and the oil film thickness of the sliding bearing can be expressed as follows:

$$h = C + y\cos\theta + x\sin\theta \tag{2}$$

3.2. Oil Film Pressure. The dynamic Reynolds equation for the radial sliding bearing in an incompressible and laminar flow state is

$$\frac{1}{r^2}\frac{\partial}{\partial\theta}\left[h^3\frac{\partial p}{\partial\theta}\right] + \frac{\partial}{\partial z}\left[h^3\frac{\partial p}{\partial z}\right] = 6\omega\eta\frac{\partial h}{\partial\theta} + 12\eta\frac{\partial h}{\partial t} \tag{3}$$

where$z$ is axial coordinate, p is lubricating oil film pressure,η is viscosity of lubricating oil (constant at an isothermal temperature), ω is rotating speed of the journal, and t is the time.

Assuming that the dimensionless variable is $H = h/C$, $(X, Y) = (x, y)/C$, $\overline{z} = z/L$, $(\ddot{X}, \ddot{Y}) = (\ddot{x}, \ddot{y})/C\omega$, $\tau = \omega t$, (3) can be nondimensionalized as follows:

$$\frac{\partial}{\partial\theta}\left[H^3\frac{\partial\overline{p}}{\partial\theta}\right] + \left(\frac{r}{L}\right)^2\frac{\partial}{\partial\overline{z}}\left[H^3\frac{\partial\overline{p}}{\partial\overline{z}}\right] = 6\frac{\partial H}{\partial\theta} + 12\frac{\partial H}{\partial\tau} \tag{4}$$

where L is the width of the sliding bearing.

The oil film pressure was solved under double Reynolds boundary conditions. That is, origin of the axial coordinate Z is the width center of the sliding bearing, and the oil film pressure at the initial boundary and fracture meets the boundary conditions given in the following equation:

$$\overline{p}\left(\theta, \overline{z} = -\frac{L}{2}\right) = \overline{p}\left(\theta, \overline{z} = \frac{L}{2}\right) = 0 \tag{5}$$

The bearing was expanded into a plane and divided into grids in the circumferential and axial directions, as shown in Figure 5, including m equal parts (numbered with i) in the θ direction and n equal parts (numbered with j) in the $\overline{z}$ direction. Each node is numbered as (i, j), with the pressure being expressed as $\overline{p}_{i,j}$. The Reynolds equation was discretized by the semistep center difference method to obtain a Reynolds pressure equation in the discrete form:

$$\overline{p}_{i,j} = \frac{A\overline{p}_{i+1,j} + B\overline{p}_{i-1,j} + C\overline{p}_{i,j+1} + D\overline{p}_{i,j-1} - F}{E} \tag{6}$$

where

$$\begin{aligned} A &= H^3_{i+1/2,j} \\ B &= H^3_{i-1/2,j} \\ C &= \frac{(r\Delta\theta)^2}{(L\Delta\overline{z})^2}H^3_{i,j+1/2} \\ D &= \frac{(r\Delta\theta)^2}{(L\Delta\overline{z})^2}H^3_{i,j-1/2} \\ E &= A + B + C + D \\ F &= 6\left(H_{i+1/2,j} - H_{i-1/2,j}\right)\Delta\theta \\ &\quad + 12\left(\dot{X}\cos\theta + \dot{Y}\sin\theta\right)(\Delta\theta)^2 \end{aligned} \tag{7}$$

Equation (6) was solved by the successive overrelaxation iteration method, in which the overrelaxation factor was 1.96. In order to achieve good results of each iteration and decide whether to terminate the iteration, the oil film pressure $\overline{p}$ of the sliding bearing was calculated with $\delta = 10^{-6}$ and (8) as the convergence criterion of iteration termination:

$$\frac{\sum_{i=2}^{m}\sum_{j=2}^{n}\left|\overline{p}^{(k)}_{i,j} - \overline{p}^{(k-1)}_{i,j}\right|}{\sum_{i=1}^{m}\sum_{j=1}^{n}\left|\overline{p}^{(k)}_{i,j}\right|} \le \delta \tag{8}$$

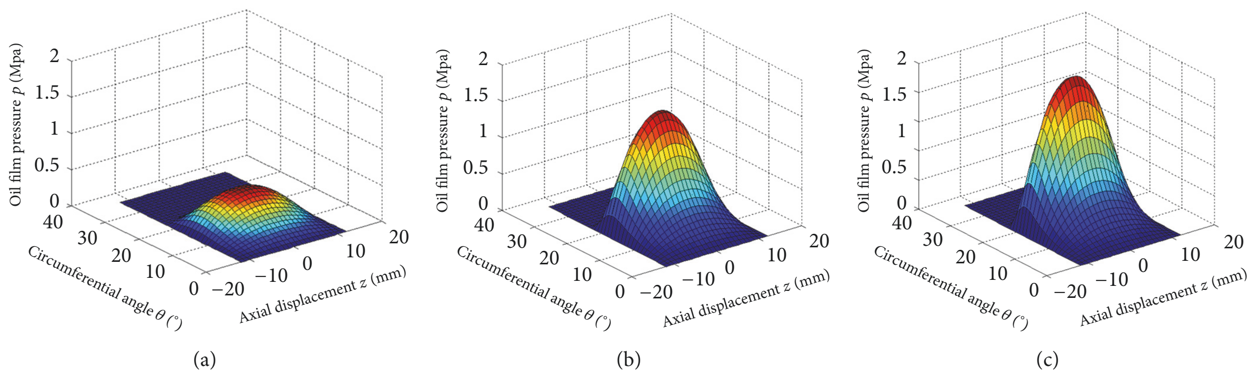

FIGURE 6: Oil film pressure of sliding bearing II under torque load. (a) 7.2 Nm, (b) 42.4 Nm, and (c) 81.5 Nm.

The resultant force of the oil film of the sliding bearing reflects the bearing capacity. The oil film pressure calculated was integrated in the x- and y-directions to obtain the components F_x and F_y of the sliding bearing of the rotor system in the x- and y-directions, respectively:

$$\begin{aligned} F_x &= \int_0^{2\pi} \int_{-L/2}^{L/2} pr \cos\theta dz d\theta \\ &= \eta L r \omega \left(\frac{r}{C}\right)^2 \int_0^{2\pi} \int_{-L/2}^{L/2} \overline{p} \cos\theta d\theta d\overline{z} = F_0 \overline{F_x} \\ F_y &= \int_0^{2\pi} \int_{-L/2}^{L/2} pr \sin\theta dz d\theta \\ &= \eta L r \omega \left(\frac{r}{C}\right)^2 \int_0^{2\pi} \int_{-L/2}^{L/2} \overline{p} \sin\theta d\theta d\overline{z} = F_0 \overline{F_y} \end{aligned} \tag{9}$$

In (9), $F_0 = \eta L r \omega (r/C)^2$; the dimensionless components $\overline{F_x}$ and $\overline{F_y}$ in the x- and y-directions, the dimensionless resultant force of the oil film, and the angle of displacement are, respectively:

$$\begin{aligned} \overline{F_x} &= \int_0^{2\pi} \int_{-L/2}^{L/2} \overline{p} \cos\theta d\theta d\overline{z} \\ \overline{F_y} &= \int_0^{2\pi} \int_{-L/2}^{L/2} \overline{p} \sin\theta d\theta d\overline{z} \end{aligned} \tag{10}$$

$$\overline{F} = \sqrt{\overline{F_x}^2 + \overline{F_y}^2} \tag{11}$$

$$\tan\phi = \frac{\overline{F_y}}{\overline{F_x}} \tag{12}$$

3.3. Simulation. The dimensionless resultant force $(\overline{F})$ and angle of displacement (ϕ) of the oil film under different torque loads can be solved by (9) and (12), with the components (see Table 3 for specific values) of the sliding bearing under five constant torque loads in the x- and y-directions, measured by the bearing load sensor. According to the relationship of the dimensionless resultant force $\overline{F}$, eccentricity ε, and angle of displacement ϕ of the oil film in [30], the radial eccentricity (ε) values under different torque loads are 0.27, 0.57, and 0.61, respectively. Then, the eccentricity e and radial center coordinates (x, y) are calculated, followed by the numerical solution of the oil film pressure by (2) and (6) and the finite difference method. The grid size of the solved area is 36×24. The pressure and thickness curves of the oil film of the sliding bearing under different torque loads can be simulated. Figures 6 and 7 show the pressure and thickness curves of the oil film of the sliding bearing II under three torque loads.

It can be seen from Figures 6 and 7 that the pressure distribution of the oil film of the sliding bearing II essentially corresponds to the thickness distribution thereof. The minimum thickness $(h_{\min})$ of the oil film is close to the outlet, and the working face where the peripheral maximum pressure of the oil film reaches the peak is on that involving the minimum thickness. Under different constant torque loads, the oil film thickness at the inlet of the sliding bearing decreases with the oil film pressure increasing and reaches the minimum value at the angle of displacement. The axial oil film thickness of the sliding bearing changes a little. When the constant torque excitation increases, the oil film fracture of the sliding bearing will move into the bearing area that gradually diminishes.

3.4. Determination of Lubrication State Based on Film Thickness Ratio. The lubrication state of the sliding bearing is determined based on the film thickness ratio Λ, i.e., the ratio of the oil film thickness to surface roughness of the friction pair of the sliding bearing. The film thickness ratio is not only a basis for classification of lubrication states of friction pairs of sliding bearings, but also an important factor affecting the friction coefficient and wear mode of the sliding bearing. Refer to the following equation for the specific solution:

$$\Lambda = \frac{h_{\min}}{\sqrt{\sigma_{\text{shaft}}^2 + \sigma_{\text{bearing}}^2}} \tag{13}$$

where $h_{\min}$ is minimum oil film thickness of the friction pair of the sliding bearing, σ_{shaft} is surface roughness of the rotating shaft, 0.0016 mm, σ_{bearing} is surface roughness of the sliding bearing, 0.0016 mm.

Based on the relationship of the friction coefficient, oil film continuity, wear rate, and film thickness ratio in [31],

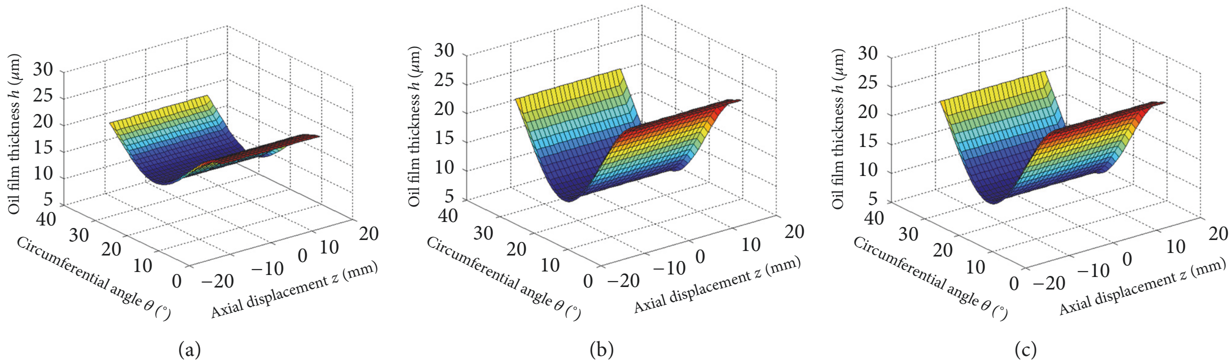

Figure 7: Film thickness of sliding bearing II under torque load. (a) 7.2 Nm, (b) 42.4 Nm, and (c) 81.5 Nm.

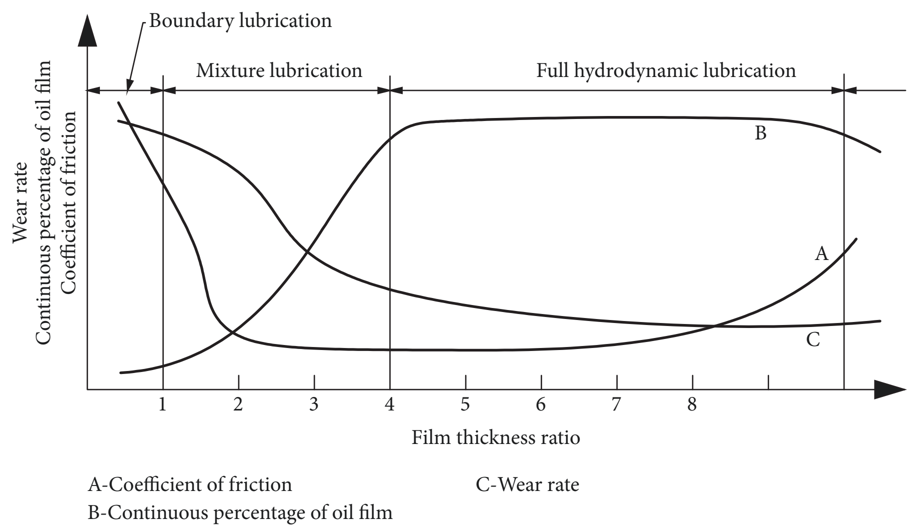

Figure 8: Relationship between wear, friction, and lubrication.

Table 4: The lubrication state of sliding bearings with different film thickness ratios.

Film thickness ratio Λ	Λ≥4	1<Λ<4	Λ≤1
Lubrication state	Full hydrodynamic lubrication	Mixture lubrication	Boundary lubrication

the lubrication states of the sliding bearing corresponding to different film thickness ratios were analyzed, as shown in Figure 8 and Table 4.

4. Results and Discussions

4.1. Effect of Torque Excitation on Change in Lubrication State of Sliding Bearing. The effect of constant torque loads on the maximum oil film pressure and minimum oil film thickness of the sliding bearing at a constant rotating speed (210 r/min) was simulated, and the lubrication state of the sliding bearing was determined based on the film thickness ratio, as shown in Table 5.

It can be seen in Table 5 that, with the constant torque increasing at a constant rotating speed, the eccentricity and maximum oil film pressure of the sliding bearing will increase, the minimum oil film thickness and the film thickness ratio will decrease, and the full fluid lubrication state will change into the mixed lubrication state. The decline in the minimum oil film thickness is caused by the movement of the rotating shaft center away from the bearing bush center with the constant torque increasing.

Figure 9 shows the curve of the film thickness ratio of the sliding bearing under torque loads, with the rotor system running at a constant speed (210 r/min). The solid line is the original curve of the film thickness ratios calculated through repeated simulation and analysis under constant torque excitation, while the dotted line is the result of fitting of the original curve. The corresponding fitting function is as follows:

$$\Lambda = 7.044 - 0.975 \ln T \tag{14}$$

Equation (14) shows that, given a constant rotating speed, the film thickness ratio of the sliding bearing of the rotor system is logarithmically related to the torque excitation. It

Table 5: Influence of different constant torque on main parameters of sliding bearing II.

Torque value (Nm)	ε	P_{max}(MPa)	h_{min}(mm)	Λ	Lubrication state
7.2	0.2747	0.467	11.61	5.13	Full hydrodynamic lubrication
21.3	0.4288	0.984	9.15	4.04	Full hydrodynamic lubrication
42.4	0.5199	1.524	7.70	3.40	Mixture lubrication
62.3	0.5740	2.025	6.84	3.02	Mixture lubrication
81.5	0.6113	2.473	6.24	2.76	Mixture lubrication

Table 6: The relationship between torque excitation and lubrication state of sliding bearing II.

Lubrication state	Range of torque (Nm)
Full hydrodynamic lubrication	$T\leq 22.69$
Mixture lubrication	$22.69<T<492.26$
Boundary lubrication	$T\geq 492.26$

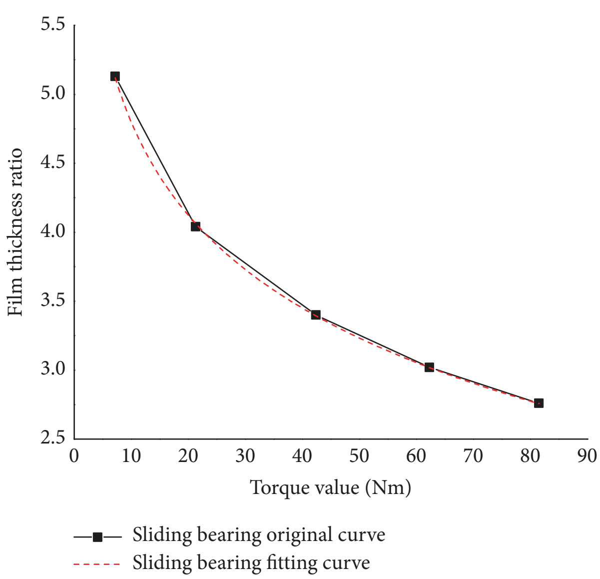

Figure 9: Film thickness ratio of sliding bearing II under different torque excitations.

can be seen from Figure 9 that, at a constant rotating speed, the film thickness ratio of the sliding bearing will decrease with the torque excitation increasing. The film thickness ratio decreases quickly within the low torque range and slowly and finally stably with the torque excitation up to a certain value.

Combining Table 3 and (14), the relationship between the torque load at the constant rotating speed (210 r/min) and the lubrication state of the sliding bearing was solved, as shown in Table 6.

4.2. Effect of Torque Excitation on Sliding Bearing Wear. The wear volume, which is an important index in the study on sliding bearing wear, can be measured in different ways. The ferrography was applied here to calculate the wear volume of the sliding bearing under constant torque loads.

The oil samples used in the sliding bearing wear test were collected from the crude oil pipe of the lubrication system, and the rotating speed of the rotor was set as 210 r/min. As the sliding bearing is worn normally, oil samples (3 ml) were collected at intervals of 5h from the return oil pipe in front of the filter, and wear particles in the oil samples were separated via the analytical ferrograph. In order to reduce experimental errors, the mass of the blank ferrogram before testing and that of the ferrogram after ferrography treatment were the averages of 10 weighing results. The mass difference of the ferrogram before and after testing is the wear volume of the sliding bearing in 3 ml lubricating oil. The concentration of wear particles of the sliding bearing can be calculated accordingly, and the wear volume of the sliding bearing within a certain period can be calculated based on the total amount of lubricating oil in the lubrication system. The specific calculation formula is as follows:

$$M = \frac{m_2 - m_1}{3} \times V \tag{15}$$

where M is the total mass of the abrasive grains in the lubrication system tank; m_1 is the average mass of the blank iron spectrum; m_2 is the average mass of the iron spectrum after the spectrum is produced; and V is the total volume of the oil in the lubrication system tank.

The wear volume results of the test are shown in Table 7.

The curve (Figure 10) of changes in the wear volume of the sliding bearing II under different torques values over time was drawn based on the test data in Table 7. It can be seen from Figure 10 that the wear volume of the sliding bearing II subjected to torque loads increases linearly over time. When the sliding bearing is in the full hydrodynamic lubrication state, its wear volume changes slowly and gradually becomes steady over time; when the sliding bearing is in the mixed lubrication state, its wear volume increases more greatly than that in the full hydrodynamic lubrication state, and the longer the time, the more greatly the sliding bearing is worn.

According to the above study, the torque loads of 7.2 Nm and 21.3 Nm correspond to the complete fluid lubrication state, and theoretically there should be no wear, but it can be seen from Figure 10 that there is still wear under these two torque excitations. This is because there is more or less eccentricity between the bearing and the journal, resulting in no complete lubrication between the friction pairs.

The wear rate curve (Figure 11) of the sliding bearing II under different torque loads was drawn based on the total wear in 20h. It can be seen that the wear rate of the sliding bearing will increase with the torque rising. The wear rate increases slowly in the full fluid lubrication state and rapidly in an exponential manner in the mixed lubrication state.

Table 7: Wear of sliding bearing II under constant torque excitation.

Torque value (Nm)	Wear of sliding bearing (mg)				
	0 h	5 h	10 h	15 h	20 h
7.2	0.12	0.14	0.17	0.20	0.24
21.3	0.13	0.17	0.21	0.26	0.31
42.4	0.13	0.19	0.25	0.32	0.39
63.2	0.14	0.22	0.31	0.40	0.50
81.5	0.14	0.26	0.40	0.53	0.66

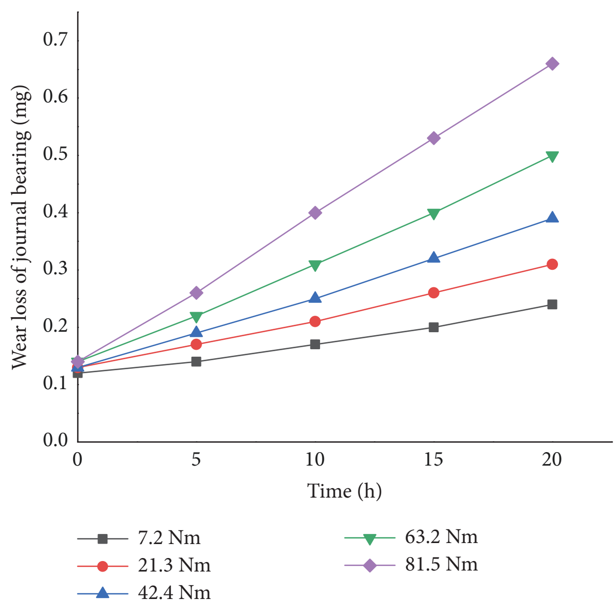

Figure 10: Time-wear curve of sliding bearing II under different torque excitations.

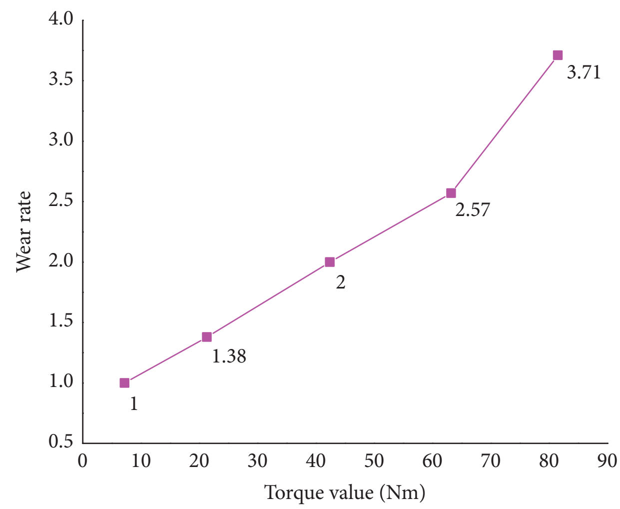

Figure 11: Wear rate of sliding bearing II under different torque loads.

4.3. Analysis of Wear Particle Morphology and Wear Mechanism of Sliding Bearing. Part of the oil samples of the sliding bearing II under five kinds of torque loads (7.2Nm, 21.3Nm, 42.4Nm, 63.2Nm, and 81.5Nm) were extracted for ferrographic analysis. The particle morphology was analyzed by amplifying 100 times, so as to study the wear mechanism of sliding bearing II under different torque loads.

Figure 12 shows the morphology of the abrasive grains under various torque excitations. The abrasive grains in (a) and (b) are arranged in a chain, but the latter has a larger abrasive grain size and a higher concentration. This wear condition corresponds to Figure 10, which verifies the correctness of the conclusion that the sliding bearing is in a fully fluidly lubricated state at $T < 22.69$Nm.

The abrasive grains in (c) have a reddish yellow color, do not obey the ferromagnetic arrangement, and have scratches on the surface, so the wear mechanism of the sliding bearing under the 42.4 Nm torque excitation is mainly abrasive wear. The surface of the abrasive grain in (d) has obvious scratches and marks and has a light blue temper color, so the abrasive particle is adhesive wear abrasive grain.

The (c) and (d) diagrams show that the sliding bearing is in a mixed lubrication state, which verifies the correctness of the conclusion that the sliding bearing will be in a mixed lubrication state when 22.69 Nm$<T<$492.26 Nm.

5. Conclusions

In this paper, the oil film pressure and thickness of the sliding bearing of the low-speed rotor system with different torque loads were calculated and simulated according to the loads measured by the bearing load sensor, followed by determination of the lubrication state of the sliding bearing under torque loads based on the film thickness ratio, and the direct relationship between the torque loads and lubrication states. The changes of wear volume and corresponding wear mechanism of sliding bearing II under different torque loads were obtained through the ferrography analysis of the oil sample, which provides a theoretical basis for further prediction and analysis of wear condition and remaining life of low-speed sliding bearings subjected to large torques in a long time. The lubrication state of high-speed sliding bearings with torque load is to be studied further. Specific conclusions are as follows:

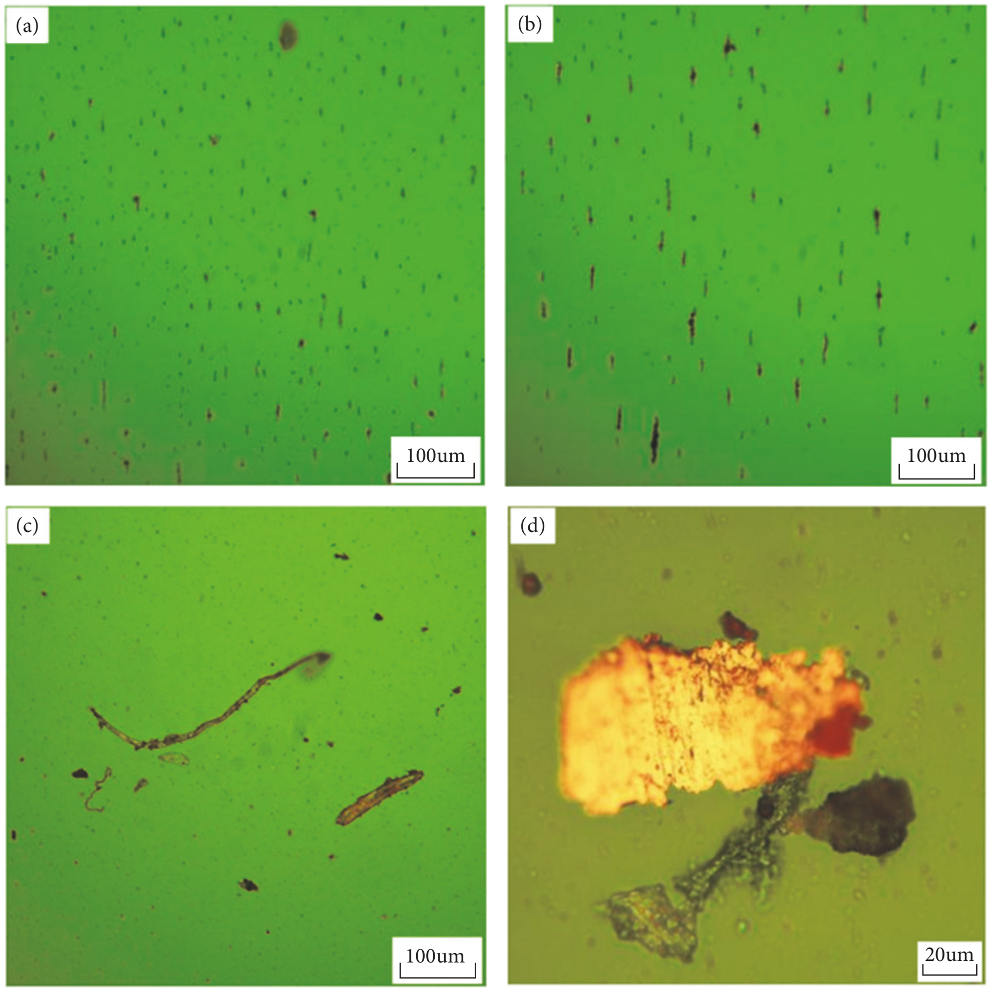

Figure 12: Abrasive grain morphology under different torque loads. (a)7.2Nm, (b)21.3Nm, (c)42.4Nm, and (d)63.2Nm.

(1) Torque values under different lubrication conditions can be determined. For the 210r/min low-speed rotor system, according to the curve of the film thickness ratio, the sliding bearing II will be in the full fluid lubrication state when the torque value is $T \leq 22.69Nm$, mixed lubrication state when the torque is $22.69Nm < T < 492.26Nm$, and boundary lubrication state when the torque is $T \geq 492.26Nm$.

(2) With the torque increasing at a constant rotating speed, the wear volume of the sliding bearing II will increase linearly over time and the wear rate exponentially. Changes in the wear rate in the mixed lubrication state are greater than those in the full fluid lubrication state.

(3) Under the condition of complete fluid lubrication, the sliding bearing II of the rotor system has no abnormal wear particles. Under mixed lubrication condition, the wear mechanism of sliding bearing II is mainly abrasive wear when torque excitation is small. With the increase of torque excitation value, the wear mechanism is mainly adhesive wear and abrasive wear.

Data Availability

The data used to support the findings of this study are available from the corresponding author upon request.

Conflicts of Interest

The authors declare that there are no conflicts of interest regarding the publication of this paper.

Acknowledgments

The authors acknowledge the financial support from the National Nature Science Foundation of China (NSFC) (51475318 and U1510116).

References

[1] Q. Fang, H. Sun, and W. Liu, "Study on the stribeck curve of slider bearing lubrication state under different load," *Journal of Mechanical Design*, vol. 1, pp. 124–126, 2016.

[2] J. Ma, C. Lu, and S. Chen, "Simulation of journal centre trajectories of hydrodynamic journal bearing under transient loads," *Journal of Vibration Measurement & Diagnosis*, vol. 30, pp. 6–10, 2010.

[3] W. Song, J. Ma, and C. Lu, "Instantaneous characteristics of slide bearing under step load," *Journal of University of Jinan (Science and Technology)*, vol. 25, pp. 392–395, 2011.

[4] W. Litwin, "Influence of local bush wear on water lubricated sliding bearing load carrying capacity," *Tribology International*, vol. 103, pp. 352–358, 2016.

[5] X. Dai, Y. Wang, and S. Yu, "Ferrographic analysis of pivot jewel bearing in oil-bath lubrication," *Wear*, vol. 376-377, pp. 843–850, 2017.

[6] X. Dai, K. Zhang, and C. Tang, "Friction and wear of pivot jewel bearing in oil-bath lubrication for high rotational speed application," *Wear*, vol. 302, no. 1-2, pp. 1506–1513, 2013.

[7] D. E. Sander, H. Allmaier, H. Priebsch et al., "Edge loading and running-in wear in dynamically loaded journal bearings," *Tribology International*, vol. 92, pp. 395–403, 2015.

[8] A. Chasalevris, F. Dohnal, and I. Chatzisavvas, "Experimental detection of additional harmonics due to wear in journal bearings using excitation from a magnetic bearing," *Tribology International*, vol. 71, pp. 158–167, 2014.

[9] J. Zhu, J. Yang, B. Sun, and Y. Yu, "Experimental research on monitoring wear of main journal bearing by using thermoelectric method in diesel engine," *Chinese Internal Combustion Engine Engineering*, vol. 35, pp. 79–84, 2014.

[10] A. Bromaghin, M. Ali, T. Ravens, T. Petersen, and J. Hoffman, "Experimental study of abrasion characteristics for critical sliding components for use in hydrokinetic devices," *Journal of Renewable Energy*, vol. 66, pp. 205–214, 2014.

[11] D. Bartel, L. Bobach, T. Illner, and L. Deters, "Simulating transient wear characteristics of journal bearings subjected to mixed friction," *Proceedings of the Institution of Mechanical Engineers, Part J: Journal of Engineering Tribology*, vol. 226, no. 12, pp. 1095–1108, 2012.

[12] T. Sano, T. Nakasone, T. Katagiri, and Y. Okamoto, "A study on wear progress of plain bearing under mixed lubrication condition," *SAE International Journal of Engines*, vol. 4, no. 1, pp. 569–580, 2011.

[13] P. G. Nikolakopoulos and C. A. Papadopoulos, "A study of friction in worn misaligned journal bearings under severe hydrodynamic lubrication," *Tribology International*, vol. 41, no. 6, pp. 461–472, 2008.

[14] T. H. Wu, J. H. Mao, G. N. Dong, H. Xu, and Y. B. Xie, "Journal bearing wear monitoring via on-line visual ferrography," *Advanced Materials Research*, vol. 44-46, pp. 189–194, 2008.

[15] E. Feyzullahoğlu and N. Şakiroğlu, "The wear of aluminium-based journal bearing materials under lubrication," *Materials and Corrosion*, vol. 31, no. 5, pp. 2532–2539, 2010.

[16] D. W. Gebretsadik, J. Hardell, and B. Prakash, "Friction and wear characteristics of different Pb-free bearing materials in mixed and boundary lubrication regimes," *Wear*, vol. 340-341, pp. 63–72, 2015.

[17] A. Pola, L. Montesano, M. Gelfi, and G. M. La Vecchia, "Comparison of the sliding wear of a novel Zn alloy with that of two commercial Zn alloys against bearing steel and leaded brass," *Wear*, vol. 368-369, pp. 445–452, 2016.

[18] Y. Zhimin, Z. Xincong, Q. Hongling et al., "Study on tribological and vibration performance of a new UHMWPE/graphite/NBR water lubricated bearing material," *Wear*, vol. 332-333, pp. 872–878, 2015.

[19] C. Chen, Y. Kang, and C. Huang, "The influences of orifice restriction and journal eccentricity on the stability of the rigid rotor-hybrid bearing system," *Tribology International*, vol. 37, no. 3, pp. 227–234, 2004.

[20] C. Chen, Y. Chang, H. Lee, Y. Wang, and Y. Kang, "The influences of capillary restriction and journal eccentricity on the stability of the rigid rotor-hybrid bearing system," *Industrial Lubrication and Tribology*, vol. 59, no. 1, pp. 46–51, 2007.

[21] A. Karkkainen, M. Helfert, B. Aeschlimann, and A. Mikkola, "Dynamic analysis of rotor system with misaligned retainer bearings," *Journal of Tribology*, vol. 130, no. 2, pp. 1–10, 2008.

[22] H. W. Li, W. T. Yu, Y. P. Fan, and S. Q. Liu, "Influence of retainer bearing misalignment on the performance of active magnetic bearing," *Advanced Materials Research*, vol. 588-589, pp. 141–146, 2012.

[23] D. Lu, J. Zhang, B. Lu, and K. Liu, "Effects of parallel misalignment on performance of hydrodynamic-rolling hybrid bearing," in *Proceedings of the ASME 2012 International Mechanical Engineering Congress and Exposition, IMECE 2012*, pp. 995–1002, USA, November 2012.

[24] J. F. Fu, K. Li, H. C. Li, K. Peng, and X. W. Liu, "Optimization design of fuel pump sliding bearing based on the analysis of lubrication characteristics," *Journal of Tribology*, vol. 3, pp. 512–520, 2018.

[25] J. Yuan, X. Pang, Z. Yang, and X. Jin, "Study on modeling and experimental of the rotor-bearing system with torque excitation," *Machinery Design and Manufacture*, vol. 7, pp. 61–64, 2016.

[26] W. Zhang, Z. Yang, G. Song, and F. Wang, "Experimental identification of transient torque fault based on bearing load," *Mechanical Science and Technology for Aerospace Engineering*, vol. 33, pp. 18–21, 2014.

[27] X. Pang and Z. Yang, "Analysis of coupled vibration between rotor system supporting on bearing load," *Journal of Vibration Measurement & Diagnosis*, vol. 33, pp. 862–867, 2013.

[28] G. Song, Z. Yang, C. Ji, and F. Wang, "Theoretical–experimental study on a rotor with a residual shaft bow," *Mechanism and Machine Theory*, vol. 63, pp. 50–58, 2013.

[29] H. Sun, Z. Yang, Q. Liang, and X. Pang, "Transverse vibration response of rotor system under mutational torque excitation," *Journal of Vibration Measurement & Diagnosis*, vol. 31, pp. 622–625, 2011.

[30] L. Xu, *Dynamic Design of High Speed Rotating Mechanical Shafting*, National Defense Industry Press, Beijing, China, 1994.

[31] M. Qiu, L. Chen, and Y. Li, *Bearing Tribology Principle and Application*, National Defense Industry Press, Beijing, China, 2012.